INTERNATIONAL JOURNAL FOR NUMERICAL METHODS IN BIOMEDICAL ENGINEERING
Int. J. Numer. Meth. Biomed. Engng. 2013; **29**:988–999
Published online 26 December 2012 in Wiley Online Library (wileyonlinelibrary.com). DOI: 10.1002/cnm.2527

COMPUTATIONAL METHODS FOR BIOMEDICAL IMAGE PROCESSING AND ANALYSIS

Monte Carlo simulation of PET images for injection dose optimization

Jiří Boldyš [1,*,†], Jiří Dvořák [1], Magdaléna Skopalová [2] and Otakar Bělohlávek [2]

[1] *Institute of Information Theory and Automation, Academy of Sciences of the Czech Republic, Pod Vodárenskou věží 4, 182 08 Praha 8, Czech Republic*
[2] *Na Homolce Hospital, PET-Center, Roentgenova 2/37, Czech Republic*

SUMMARY

When a patient is examined by positron emission tomography (PET), radiotracer dose amount (activity) has to be determined. However, the rules for activity correction according to patients' weight used nowadays do not correspond with practical experience. Very high image quality is achieved for slim patients, whereas noisy images are produced for obese patients. There is opportunity to modify the correction rule with the aim to equalize image quality within the broad spectrum of patients and to diminish radiation risk to slim patients, with special importance for children.

We have built a model of a particular PET scanner and approximated human trunk, which is our region of interest, by a cylindrical model with segments of liver, outer adipose tissue, and the rest. We have performed Monte Carlo simulations of PET imaging using the GATE simulation package. Under reasonably simplifying assumptions and for special parameters, we have developed curves that recommend amount of injected activity based on body parameters to give PET images of constant quality, the quality being expressed in terms of noise equivalent counts. The dependence qualitatively differs from the rules used in clinical practice nowadays, and the results indicate potential for improvement. Copyright © 2012 John Wiley & Sons, Ltd.

Received 15 February 2012; Revised 15 October 2012; Accepted 16 October 2012

KEY WORDS: positron emission tomography; Monte Carlo simulation; biological system modeling; image quality

1. INTRODUCTION

Positron emission tomography (PET) is a functional imaging modality. Resulting images display functional processes in a patient body depending on radiotracer used, for example, glucose metabolism. These examinations allow us to localize cancer, assess tumor treatment, and so forth. For a detailed discussion on PET, see, for example, [1].

Positron emission tomography imaging is based on injecting radioactive tracer. For activities used in clinical practice, resulting image quality grows with injected activity amount. The dose amount recommendation used nowadays depends linearly on the patient's weight-the European Association of Nuclear Medicine (EANM) guidelines [2]. An exception is the specific recommendation for children that tries to equalize effective radiation dose among the patients (the EANM pediatric dosage card [3]). However, these recommendations do not sufficiently normalize for image quality in daily routine. Slim patients are given unnecessary amount of radiotracer, and obese patients would need more activity to produce images of sufficient quality. Figure 1 shows examples of computed tomography (CT) and PET images of slim and obese patients.

*Correspondence to: Jiří Boldyš, Institute of Information Theory and Automation, Academy of Sciences of the Czech Republic, Pod Vodárenskou věží 4, 182 08 Praha 8, Czech Republic.

†E-mail: boldys@utia.cas.cz

Copyright © 2012 John Wiley & Sons, Ltd.

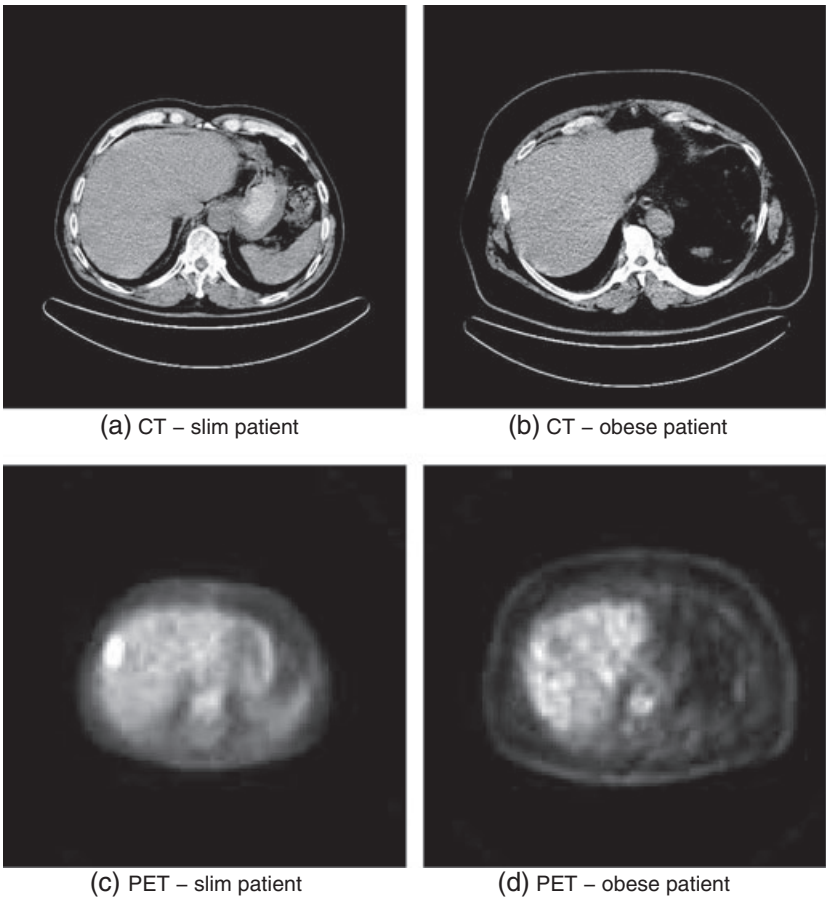

Figure 1. Computed tomography (CT) images of similar transverse plane containing liver—gray homogeneous region on the left. Reader can observe different thickness of the subcutaneous adipose tissue for a slim (a) and an obese (b) patient. Images (c) and (d), resp., show corresponding sections of positron emission tomography (PET) images. Hot spot on the (c) image represents glucose hypermetabolism typical for cancer metastasis in the liver.

Previous studies published in literature aimed at achieving maximum quality of the resulting image for each patient. However, this again leads to excess radiation exposure of light patients. A brief overview of these studies, together with different metrics of image quality they use, is presented in Section 2.

The goal of this paper is different—to qualitatively determine, based on significant patient body parameters, the amount of injected radiotracer needed to achieve constant quality of the resulting PET images, even for patients with different body habitus. This would help improve consistency of the diagnostic process. To our best knowledge, this is a novel approach to injection dose optimization in PET and we are not aware of any other published work that could be directly compared with our results.

This paper describes results of our initial study in this direction. At the beginning of our research, we have adopted several justifiable simplifications explained further on. We limit ourselves to examination of liver and body segment surrounding it. The objective of this paper is rather general—achieving constant quality. We do not study here any particular medical application domain, although we elaborate on it elsewhere—for example, lesion detectability [4].

To achieve our objectives, we have performed Monte Carlo simulations of PET imaging. Details, including description of PET scanner and body model, will follow in relevant sections. We will also explain the adopted image quality measure. Finally, we come to the desired curves that we call curves of constant quality.

Copyright © 2012 John Wiley & Sons, Ltd.

DOI: 10.1002/cnm

2. INJECTION DOSE OPTIMIZATION—PREVIOUS STUDIES

This section provides a brief (and certainly not complete) overview of studies concerning optimization of injection dose in PET. Note that all the listed studies, unlike ours, aimed at maximizing the image quality.

A popular tool for describing quality of PET images is the noise equivalent count, NEC (for detailed description, see Section 6). Studies using NEC to describe PET image quality or modeling the dependence of NEC on the amount of injected activity were published in the past few years [5–9].

Quality of reconstructed images can be also expressed in terms of signal-to-noise ratio [8, 10]. Other possibility is to assess the subjective visual quality of the images using a numeric scale or verbal description (rating the quality, e.g., from excellent to nondiagnostic). This type of psychophysical measurement is usually very time-consuming because the set of analyzed images has to be assessed by one or more experienced physicians [11, 12].

The ultimate measure of PET image quality, from the medical point of view, is performance of a human observer in a given diagnostic task. The most common task is the detection of small foci of increased activity indicating the presence of a tumor (lesions). Again, human observer studies are time-consuming, and so mathematical model observers were developed to mimic the performance of human observers in a specific task. The most important of these observers are Hotelling and channelized Hotelling observer and their variants [12–14].

3. RADIOTRACER DOSE IN POSITRON EMISSION TOMOGRAPHY IMAGING

Positron emission tomography examination is useful, for example, for tumor imaging. Tumors accumulate glucose more than surrounding tissues. Therefore, patient is in advance injected a dose of ^{18}F-fluorodeoxyglucose (^{18}F-FDG), what is a radioactive analog of glucose. ^{18}F-FDG is accumulated into tumor, and it is emitting positrons. Positrons almost immediately annihilate, resulting in two photons moving in opposite directions and detected approximately at the same time. Reconstructed image is based on number of detected photon pairs and their lines of response (LORs—lines joining two detector segments which detected the photons in coincidence)—see Figure 2 presenting PET scanner scheme.

There are standard recommendations on what amount of activity A should be injected into patient. The EANM guidelines recommend that for ^{18}F-FDG and fixed scan duration of 5 min per bed position, approximately 2.5 MBq/kg ($\pm 10\%$) is applied in the case of three-dimensional scans. Alterations of this protocol according to the bed overlap are also given in the guidelines [2].

According to the EANM guidelines, for children under 19 years, ^{18}F-FDG activity must conform to the EANM pediatric dosage card [3]. For ^{18}F-FDG PET examinations, it recommends that

$$A = \text{constant} \cdot \left(\frac{m}{70}\right)^{0.8634},$$

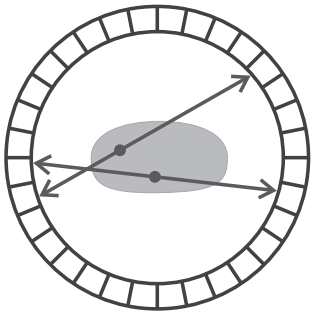

Figure 2. Positron emission tomography modality scheme showing the detector ring, annihilation events (dots), and pairs of photons moving in opposite directions (with their respective lines of response).

Copyright © 2012 John Wiley & Sons, Ltd.

DOI: 10.1002/cnm

where constant is chosen according to the type of PET scanner and other factors. Thus, specific activity of the radiopharmaceutical in the patient's body decreases with lower body weight. At the same time, higher weight demands higher activity, because heavier patients usually have more adipose tissue what implies lower probability to detect incidences of photon pairs and finally image of worse quality.

PET scanner detectors register not only true coincidences, where the photons travel from the annihilation point to the detectors without any interaction. It also happens that photons interact by Compton effect with the tissue and deflect. More tissue may increase the probability of Compton effect causing wrong LOR attributions—scattered coincidences. Furthermore, the so-called random coincidences occur when two photons from two different annihilations are detected at the same time. Scattered and random coincidences have undesirable effect on the resulting image. They introduce blurring and noise to the data.

Numbers of all coincidences grow with increasing activity. However, random coincidence count grows the fastest, causing image quality to deteriorate above some injected activity. This means that for obese patients with high amounts of injected activity, we might not be able to obtain image of sufficient quality. Typical dependencies of true, scattered, and random coincidence counts on the amount of injected activity can be found later in Figures 6–8.

The activity of radiotracer applied in a PET examination determines the radiation dose received by the patient. For example, it is approximately 0.02 mSv/MBq of ^{18}F-FDG according to International Commission on Radiological Protection (ICRP) publication 106 [15]. It means that patients of different weights are given dose of approximately 4–8 mSv. If the combined PET/CT examination is performed, additional radiation dose is received from the CT. The effective CT dose could range from 1 to 20 mSv and may be even higher for high-resolution diagnostic CT scan [2]. In this paper, we focus on optimization of the amount of radiotracer used in PET examination and thus of the radiation dose from the radiotracer, and disregard the dose from the possible CT scan.

The resulting image quality depends strongly on the duration of the scan. One may decide to apply higher activity and reduce the duration of the scan or, preferably, use reduced activity and increase scan duration, thereby keeping ALARA principles in mind [2]. In this paper, we assume that the scan duration is fixed and focus on the amount of the applied radiotracer.

4. MONTE CARLO SIMULATIONS

The process of PET imaging can be modeled by Monte Carlo methods. There are several simulation packages available for this purpose. We have chosen the GATE simulation package [16]. GATE is an open-source software and currently it is able to simulate PET, single-photon emission CT, and CT imaging. GATE is developed by OpenGATE collaboration.

The main GATE component is the Geant4 toolkit for the simulation of the passage of particles through matter. It allows us to model usual particle physics interactions, such as Compton or Rayleigh scattering, and so forth.

GATE performs PET imaging simulation after specifying the following: PET scanner model, phantom model (in our case body model), source model, time of examination, and eventually other data.

Siemens Biograph40 TruePoint TrueV HD PET scanner (Siemens AG, Erlangen, Germany) is modeled in this study. It is a cylindrical type of scanner (Figure 3). Important parameters of the scanner are as follows: detector material LSO, detector ring diameter 842 mm, four detector rings, 192 detector blocks, 169 crystals per detector blocks, crystal dimensions $4.0 \times 4.0 \times 20$ mm, axial field of view 216 mm, and coincidence window 4.5 ns. Energy window for photon detection used in the simulation was 425–650 keV as used for this scanner in Na Homolce Hospital, Prague. Simulated acquisition time was 60 s.

5. PATIENT MODEL

For general PET imaging simulations, an elaborate full body model would find its use. Our first objectives are rather qualitative, and thus, we can afford a very simplified body model at this stage.

Copyright © 2012 John Wiley & Sons, Ltd.

DOI: 10.1002/cnm

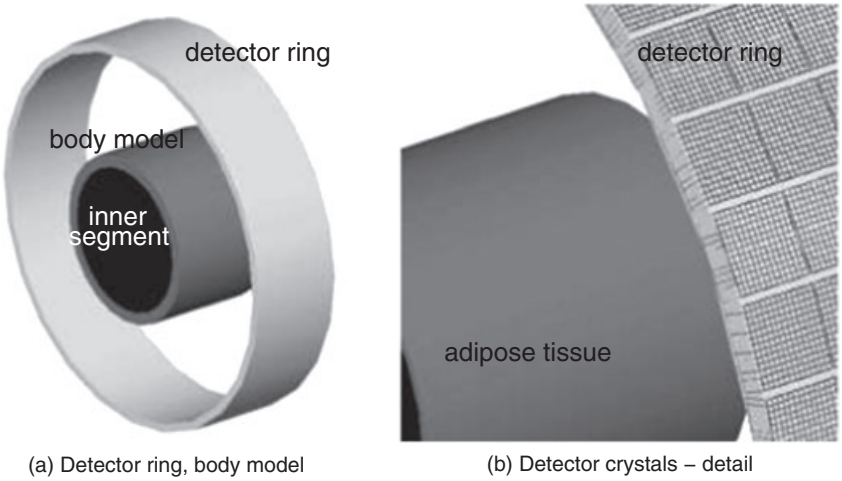

Figure 3. Model of our studied positron emission tomography scanner together with the body region of interest used in GATE simulations. (a) the whole setup and (b) detail. In the body model, adipose tissue and the inner segment are visible. Liver is hidden inside and it is not visible.

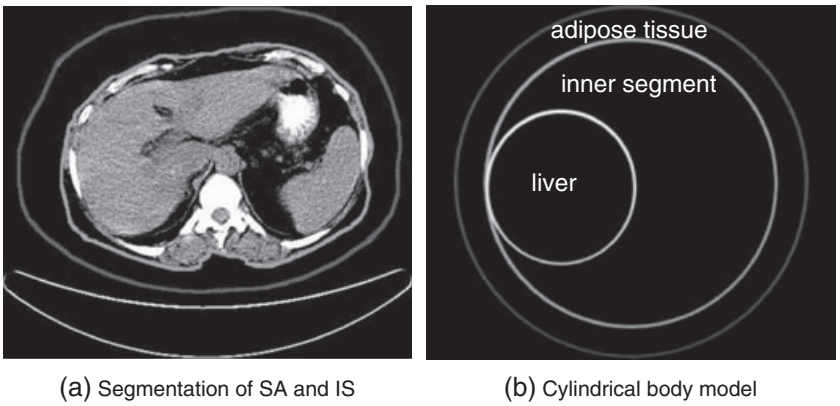

Figure 4. (a) Computed tomography images were segmented to obtain the subcutaneous adipose tissue (SA) and everything else inside SA (IS) segments. Their areas are basis of the equivalent cylindrical model (b).

In this paper, we choose liver as our main region of interest. Thus, we confine ourselves to the trunk area surrounding liver with some overlap.

We further construct a simplified cylindrical model of a transverse section through a body in liver area. We segment the section into three areas: subcutaneous adipose tissue SA (underskin fat), liver LI, and everything else inside SA, what we call inner segment IS (Figure 4(a)). We have a database of 18 CT images of slim to obese patients, where we have localized one reference transverse section on the basis of liver shape. The three defined segments were then manually segmented, and areas of segments SA and IS were measured. These areas were then recalculated into effective radii R_{SA} and R_{IS} of corresponding cylinder bases (i.e., the radii of circles having the same area as segments SA and IS).

On our limited set of CT images, radii R_{SA} and R_{IS} can be statistically explained using linear regression. We initially focus only on male patients because of different way of fat deposition. The difference was also noticeable in the dependence of R_{SA} and R_{IS} on the patient's body parameters.

Explanatory variables in the regression analysis available from the records of patient's examination are

Copyright © 2012 John Wiley & Sons, Ltd.

DOI: 10.1002/cnm

- m—patient's weight in kilograms,
- h—height in meters,
- T—age in years.

We also consider two variables derived from them: the body mass index BMI and an artificial variable x, which are defined as

$$\mathrm{BMI} = \frac{m}{h^2}, \quad x = \sqrt{\frac{m}{h}}.$$

Motivation for introducing the variable x was in considering how the body weight depends on its proportions.

In regression analysis for R_{SA}, we start from the complete model involving all the available explanatory variables:

$$R_{\mathrm{SA}} = \beta_0 + \beta_1 m + \beta_2 h + \beta_3 T + \beta_4 \mathrm{BMI} + \beta_5 x + \epsilon,$$

where ϵ is the error term and $\beta_0, \ldots, \beta_5$ are regression coefficients.

We successively remove the terms with estimated coefficients close to zero (not significant at 5% significance level). On the basis of the analysis of residuals in the models, we do not reject normality and independence of residuals.

This leads us eventually to the following simple model:

$$R_{\mathrm{SA}} = 8.21 + 21.7 \cdot x + \epsilon.$$

The term x is significant at significance level $< 10^{-5}$. Coefficient of determination in this model is $R^2 = 0.9484$. It means that this model describes the variability of the effective radii very well, and introducing the artificial explanatory variable x was a legitimate step. However, the results are based on a relatively small number of observed values.

Analogous analysis of R_{IS} results in the following model:

$$R_{\mathrm{IS}} = -39.3 - 3.21 \cdot \mathrm{BMI} + 39.2 \cdot x + \epsilon,$$

where ϵ is again the error term. Coefficient of determination in this model is $R^2 = 0.903$. Both x and BMI are significant on 5% significance level (resulting p-values are 0.0047 and 0.0281 for x and BMI, respectively) even though applying scaling law both are of linear dimension. If either x or BMI is dropped from the model, the coefficient of determination drops considerably.

This enables us to describe R_{SA} and R_{IS} in terms of patient's weight m and height h only. To further simplify the simulations, we set $h = 1.80$ m, and we vary only the weight m.

Cylindrical model of patient's trunk is then constructed as follows (Figure 4(b)). Cylinder with height 25 cm and radius R_{IS} models the inner segment. It is surrounded by another cylindrical layer with radius R_{SA}, which models the SA segment. Liver is modeled by a sphere with radius $R_{\mathrm{IS}}/2$ touching the far left point of the IS segment. The radii R_{SA} and R_{IS} depend on the parameter m and are determined according to the linear regression model described previously. Such kind of a simple model was found sufficient to approximate body region of interest for PET imaging simulations.

Materials for all the segments were appropriately chosen from the GATE material database (*Adipose* for the SA segment and *Liver* for both the IS and LI segment as the chemical composition of the internal organs is very similar). As for the distribution of activity in the model of patient's trunk, we chose homogeneous distribution in all the segments SA, LI, and IS. The ratios of volume activity (activity per cubic centimeter) in different segments correspond to average ratios determined from PET images of real patients for which both PET and CT images were available.

In a CT image, the individual segments were determined, and from the corresponding parts of PET images, the mean number of counts per cm^3 (i.e., the volume activities, denoted by $a_{\mathrm{SA}}, a_{\mathrm{IS}}$, and a_{LI}, respectively) was calculated.

By taking ratios of these volume activities $a_{\mathrm{IS}}/a_{\mathrm{SA}}$ and $a_{\mathrm{LI}}/a_{\mathrm{SA}}$, we obtained quantities independent of the acquisition time and thus comparable among different patients. Average ratios $a_{\mathrm{IS}}/a_{\mathrm{SA}}$ and $a_{\mathrm{LI}}/a_{\mathrm{SA}}$ and their standard deviations for the given set of patients were found to be 2.4 ± 0.7 and 5.6 ± 1.4, respectively.

Copyright © 2012 John Wiley & Sons, Ltd.

DOI: 10.1002/cnm

6. IMAGE QUALITY ASSESSMENT

There are many image quality measures available in the field of image analysis. Overview of such measures suitable for PET imaging was given in Section 2. For the purpose of this paper, the NEC was chosen. NEC is for a uniform cylinder proportional to the square of the resulting signal-to-noise ratio in an analytically reconstructed image [17]. It is a very simple measure and at the same time it is widely used in nuclear medicine community.

Noise equivalent count quantifies the statistical quality of the raw data prior to reconstruction and thus is not affected by the choice of reconstruction algorithm. In fact, no tomographic reconstruction was needed for this study.

Noise equivalent count is based on the total numbers of true coincidences T, scattered coincidences S, and random coincidences R. Data for NEC calculation are available from outputs of our simulations. The defining relation is

$$\mathrm{NEC} = \frac{T^2}{T + S + fR},$$

where f is the fraction the phantom or patient occupies in the scanner's field of view [6].

If t is the length of the acquisition (in seconds), one could also define NEC rate as

$$\text{NEC rate} = \frac{(T/t)^2}{T/t + S/t + fR/t}.$$

The resulting NEC rate is independent of the acquisition time t if the coincidence count rates (counts per second) T/t, S/t and R/t are fixed. It holds that NEC $= t \cdot$ NEC rate. However, in this paper, we focus on NEC rather than NEC rate.

Because of behavior of dependencies of T, S, and R on activity A mentioned in Section 3, dependence NEC(A) is first growing and then decreasing.

7. SIMULATION RESULTS

We have performed PET imaging simulations with the PET scanner model and the patient body model described earlier. For simplicity and as mentioned previously, we were varying only the weight parameter m.

We simulated trunks of six patients (denoted A–F) with different weights evenly distributed in the range from 48 to 130 kg. From the given weight and default height 1.80 m, we calculated parameters R_{SA} and R_{IS} needed to specify the patient body model.

The range of activities used in simulations was chosen so that it covers the activities that would be given to the model patients in PET center of Na Homolce Hospital, Prague, where the prescribed amount of activity in megabecquerels (MBq) is

$$A = 290 \cdot \left(\frac{m}{70}\right)^{0.8634},$$

that is, the recommendation given by the EANM pediatric dosage card extrapolated for the whole range of patient weights. The resulting interval of activities is [190, 540] MBq, which covers the relevant values with approximately 10% overlap at both ends.

Body parameters of the considered patients together with the calculated parameters are summarized in Table I. In this study, we performed for each patient 15 independent PET imaging simulations with activities systematically covering the whole interval [190, 540] MBq. NEC was then computed for every simulation based on T, S, and R. Results are plotted in Figure 5.

Resulting dependence NEC(A) can be fitted by a curve $\mathrm{NEC}(A) = p_1 + p_2 A^{p_3}$, where p_is are fitted parameters. The estimated values of p_3 for the six patients are close to 0.8, that is, smaller than one meaning that the increase in NEC is lower than linear. This is caused by the faster-than-linear growth of the number of random coincidences with increasing activity and only slightly

Copyright © 2012 John Wiley & Sons, Ltd.

DOI: 10.1002/cnm

Table I. Simulation parameters: patients' body parameters (weight, height, and body mass index), dimensions of the corresponding phantoms (R_{SA} and R_{IS}), and the amount of applied activity A according to [3] (in megabecquerels).

Patient	m (kg)	h (m)	BMI	R_{SA} (mm)	R_{IS} (mm)	A (MBq)
A	48.6	1.80	15.0	121	116	212
B	64.8	1.80	20.0	139	132	271
C	81.0	1.80	25.0	154	144	329
D	97.2	1.80	30.0	168	153	385
E	113.4	1.80	35.0	181	160	440
F	129.6	1.80	40.0	193	165	494

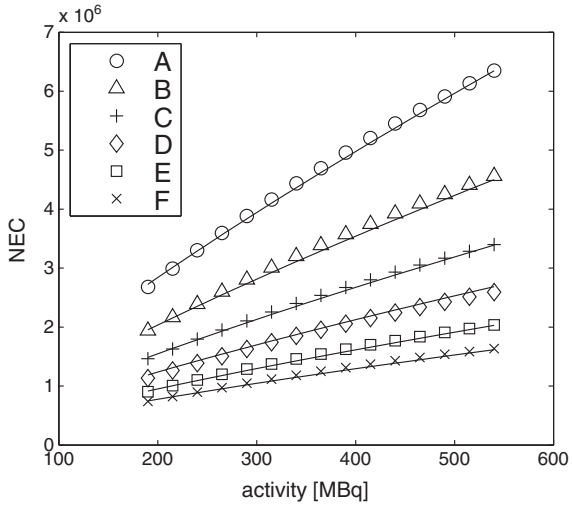

Figure 5. Dependence of noise equivalent count (NEC) image quality measure on simulated activity for the six considered patient models.

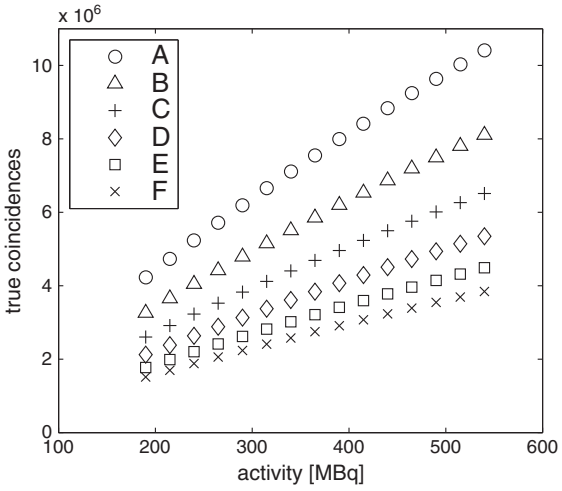

Figure 6. Dependence of the number of true coincidences on applied activity for patients with different weights.

sublinear growth (due to the imaging process) of the numbers of true and scattered coincidences. Dependence of the true, scattered, and random coincidence counts on the amount of injected activity is plotted in Figures 6–8, respectively.

Copyright © 2012 John Wiley & Sons, Ltd.

DOI: 10.1002/cnm

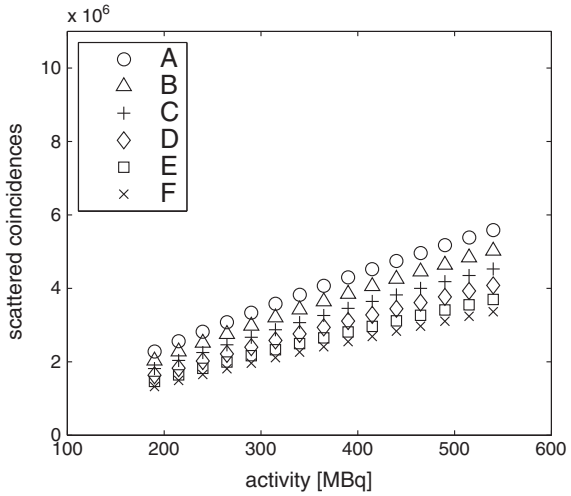

Figure 7. Dependence of the number of scattered coincidences on applied activity for patients with different weights.

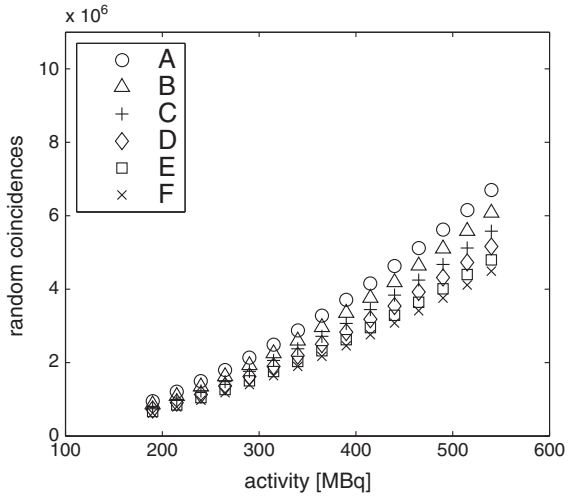

Figure 8. Dependence of the number of random coincidences on applied activity for patients with different weights.

The resulting curve $\mathrm{NEC}(A) = p_1 + p_2 A^{p_3}$ can be used to propose activity A, which has to be used to achieve a desired reference level of NEC. Such activities are plotted in Figure 9. Different symbols correspond to different reference levels of NEC. Solid line shows the prescription used today in Na Homolce Hospital, Prague.

It is evident from Figure 9 that the dependence of injected activity on body parameters is qualitatively different from the prescription used nowadays. The resulting curves of constant quality (interpolated through the marks) show rather convex tendency on the contrary to today's linear [2] or sublinear [3] standard.

The results support observations from clinical practice. It seems that there is potential to save slimmer patients from radiation load, what is crucial for reducing the potential risk of radiation-induced cancer by PET investigation. On the other hand, we developed a methodology capable of finding suitable activities for simulated obese patients to obtain clinically informative PET images.

Copyright © 2012 John Wiley & Sons, Ltd.

DOI: 10.1002/cnm

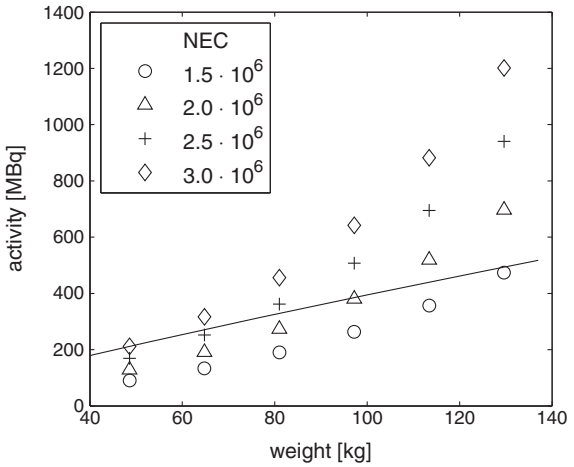

Figure 9. Prescription of applied activity based on patient weight. Different symbols correspond to different reference values of noise equivalent count (NEC). For example, circles determine the amount of activity that would produce images with NEC $= 1.5 \cdot 10^6$. Solid line—activity injected in Na Homolce Hospital, Prague (EANM pediatric dosage card extrapolated to the whole range of patient weight).

8. DISCUSSION

Computer simulations were chosen as a starting point of the dose optimization study. They allowed us to work with range of activities that would not be medically justifiable for patients in the everyday practice.

Among different body parts, we have chosen the region of liver because of the following reasons. Liver is an organ with frequent occurrence of metastases. In the liver, there is physiologic increased glucose metabolism, thus small cancerous hypermetabolic foci are hardly to be differentiated from the noise, especially when image noise significantly varies among patients. The liver is large enough to facilitate standardization of measurement on patients when results of our work would be tested in clinical practice.

The set of CT images that were used in Section 5 to determine the phantom proportions is somewhat limited. The models correspond to male patients, and thus, the results are not directly applicable to female patients. However, we expect shape of the curves of constant quality for female patients to be similar to those shown in Figure 9.

Acquisition time for PET imaging in practice is usually 180 seconds per bed position (one position of the patient in the scanner). Because of the dimensions of the constructed patient model and the scanner's field of view, it is sufficient for our study to use only one bed position.

Because the coincidence events are distributed almost evenly along the time interval of acquisition and the coincidence counts in disjoint time intervals are independent, we have found that it is enough to simulate only 60 s of the acquisition. Longer acquisition time would change the NEC values by a multiplicative constant, and the results would be qualitatively the same. Of course, in practice, it is reasonable to increase the acquisition time in order to improve image quality (doubling the acquisition time approximately doubles resulting NEC) rather than increase the radiotracer dose (doubling the dose does not double resulting NEC, Figure 5), especially for heavy patients. However, in this study, we focus on qualitative results for a fixed acquisition time.

As for the decrease of activity during acquisition, we can either neglect it (during the 3 min of acquisition less than 2% of ^{18}F-FDG decay) or realize that it affects the NEC values only by a multiplicative constant.

Other measures of PET image quality may be used in this type of study. Apart from the classical measures mentioned in Section 2, in another paper, we proposed a new mathematical method of expressing the image quality in terms of lesion detectability [4]. The method makes use of the

Copyright © 2012 John Wiley & Sons, Ltd.

DOI: 10.1002/cnm

results of random field theory and integral geometry. Although the study of lesion detectability is out of the scope of this paper, we briefly recall the main idea of this approach.

In certain situations, PET images can be regarded as realizations of a smooth random field sampled on a rectangular lattice of discrete points. The diagnostic task of detecting lesions in a homogeneous tissue (e.g., liver) can be thought of as detecting significant increase of the random field's values. This task can be treated as a problem of testing null hypothesis that the random field has a constant mean.

Under specific assumptions about the random field's distribution, a threshold value can be determined, which is exceeded by the values of the random field only with a given probability (say 0.05)—for example, [18]. Then, following the standard procedure of hypothesis testing, one can reject the null hypothesis of constant mean if the values of the random field exceed the threshold at any point. This leads to the conclusion that significant activation (increase of the random field's values) is present in the image. Moreover, the activation can be easily localized—it is situated at the points at which the values exceed the threshold.

A study deriving the curves of constant quality using this method of lesion detection [4] confirms the qualitative results presented in this paper. However, the method itself has only a limited use in diagnostics of lesions due to its assumption of homogeneity of the inspected tissue.

As mentioned in Section 6, we do not reconstruct the simulated tomographic data to obtain simulated reconstructed PET images in this paper. Monte Carlo simulations in GATE simulation package allow us to know the ground truth about the underlying processes in PET imaging. We know which events resulted in true, scattered, or random coincidences. Because numbers of these events are sufficient to calculate the NEC image quality measure, there is no need to reconstruct the images. We recognize that for particular applications, different reconstruction algorithms have different impacts on the image content critical in medical examination. Because we limit ourselves to qualitative results here, we can view the data we use as of those resulting from an ideal reconstruction algorithm and thus general and invariant to degradations specific to particular reconstruction algorithms.

Depending on the chosen reference image quality, activities proposed here for obese patients might be higher than what is prescribed nowadays. The weight scale will be most probably divided into intervals where we propose lower activities for the interval with lower weights, and vice versa. We see eventual benefits for the obese patients as (i) standardization of the examinations and thus easier comparability of examinations from medical databases and (ii) PET imaging containing useful information about patient's condition.

The results presented in this paper confirm results of our preliminary study [19], where activities were chosen randomly from the given interval.

9. CONCLUSIONS

We have achieved the main goal of this study—we have derived curves of constant quality that qualitatively predict the amount of injected radiotracer to produce resulting PET image of constant quality for particular body parameters. The results support clinical experience of physicians from the PET Center of Na Homolce Hospital.

Our plans for the future include elaboration of more realistic body model. We will also further investigate other image quality measures and impact of the reconstruction process.

ACKNOWLEDGEMENTS

We are very grateful to Filip Šroubek (Institute of Information Theory and Automation, AS CR), Pavel Máca (Na Homolce Hospital, Prague), and Radek Matějka (Siemens Czech Republic) for fundamental technical help. We also thank the OpenGATE Collaboration for GATE development.

This work has been supported by the Czech Ministry of Education under the project no. 1M0572 (Research Center DAR).

Copyright © 2012 John Wiley & Sons, Ltd.

DOI: 10.1002/cnm

REFERENCES

1. Powsner RA, Powsner ER. *Essential Nuclear Medicine Physics*. Wiley-Blackwell: Malden, Massachusetts, USA, 2006. DOI: 10.1002/9780470752890.
2. Boellaard R, O'Doherty MJ, Weber WA, Mottaghy FM, Lonsdale MN, Stroobants SG, Oyen WJG, Kotzerke J, Hoekstra OS, Pruim J, Marsden PK, Tatsch K, Hoekstra CJ, Visser EP, Arends B, Verzijlbergen FJ, Zijlstra JM, Comans EFI, Lammertsma AA, Paans AM, Willemsen AT, Beyer T, Bockisch A, Schaefer-Prokop C, Delbeke D, Baum RP, Chiti A, Krause BJ. FDG PET and PET/CT: EANM procedure guidelines for tumour PET imaging: version 1.0. *European Journal of Nuclear Medicine and Molecular Imaging* 2010; **37**(1):181–200. DOI: 10.1007/s00259-009-1297-4.
3. Jacobs F, Thierens H, Piepsz A, Bacher K, Van de Wiele C, Ham H, Dierckx RA. Optimised tracer-dependent dosage cards to obtain weight-independent effective doses. *European Journal of Nuclear Medicine and Molecular Imaging* 2005; **32**(5):581–588. DOI: 10.1007/s00259-004-1708-5.
4. Dvořák J, Boldyš J, Skopalová M, Bělohlávek O. Application of the random field theory in medical imaging—detecting lesions in PET images. Submitted, 2011.
5. Accorsi R, Karp JS, Surti S. Improved dose regimen in pediatric PET. *The Journal of Nuclear Medicine* 2010; **51**(2):293–300. DOI: 10.2967/jnumed.109.066332.
6. Danna M, Lecchi M, Bettinardi V, Gilardi MC, Stearns CW, Lucignani G, Fazio F. Optimization of tracer injection for 3D ^{18}F-FDG whole body (WB) PET studies using an acquisition-specific NEC (AS-NEC) curve generation. In: *2004 IEEE Nuclear Science Symposium Conference Record* 2004; **4**:2615–2619. DOI: 10.1109/NSSMIC.2004.1462788.
7. Danna M, Lecchi M, Bettinardi V, Gilardi MC, Stearns CW. Generation of the acquisition-specific NEC (AS-NEC) curves to optimize the injected dose in 3D ^{18}F-FDG whole body PET studies. *IEEE Transactions on Nuclear Science* 2005; **53**(1):86–92. DOI: 10.1109/TNS.2005.862966.
8. Mizuta T, Senda M, Okamura T, Kitamura K, Inaoka Y, Takahashi M, Matsumoto K, Abe M, Shimonishi Y, Shiomi S. NEC density and liver ROI S/N ration for image quality control of whole-body FDG-PET scans: comparison with visual assessment. *Molecular Imaging and Biology* 2009; **11**(6):480–486. DOI: 10.1007/s11307-009-0214-3.
9. Watson CC, Casey ME, Bendriem B, Carney JP, Townsend DW, Eberl S, Meikle S, DiFilippo FP. Optimizing injected dose in clinical PET by accurately modeling the counting-rate response functions specific to individual patient scans. *The Journal of Nuclear Medicine* 2005; **46**(11):1825–1834.
10. Watson CC. Count rate dependence of local signal-to-noise ratio in positron emission tomography. *IEEE Transactions on Nuclear Science* 2004; **51**(5):2670–2680. DOI: 10.1109/TNS.2004.835743.
11. Everaert H, Vanhove C, Lahoutte T, Muylle K, Caveliers V, Bossuyt A, Franken PR. Optimal dose of ^{18}F-FDG required for whole-body PET using an LSO PET camera. *European Journal of Nuclear Medicine and Molecular Imaging* 2003; **30**(12):1615–1619. DOI: 10.1007/s00259-003-1317-8.
12. Halpern BS, Dahlbom M, Auerbach MA, Schiepers C, Fueger BJ, Weber WA, Silverman DHS, Ratib O, Czernin J. Optimizing imaging protocols for overweight and obese patients: a lutetium orthosilicate PET/CT study. *The Journal of Nuclear Medicine* 2005; **46**(4):603–607.
13. Abbey CK, Barrett HH. Human- and model-observer performance in ramp-spectrum noise: effects of regularization and object variability. *The Journal of the Optical Society of America A* 2001; **18**(3):473–488. DOI: 10.1364/JOSAA.18.000473.
14. Gifford HC, King MA, de V, D J, Soares EJ. Channelized Hotelling and human observer correlation for lesion detection in hepatic SPECT imaging. *The Journal of Nuclear Medicine* 2000; **41**(3):514–521.
15. ICRP. Radiation dose to patients from radiopharmaceuticals. Addendum 3 to ICRP Publication 53. ICRP Publication 106. Approved by the Commission in October 2007. *Annals of the ICRP* 2008; **38**(1-2):1–197. DOI: 10.1016/j.icrp.2008.08.003.
16. Jan S, Santin G, Strul D, Staelens S, Assie K, Autret D, Avner S, Barbier R, Bardies M, Bloomfield PM, Brasse D, Breton V, Bruyndonckx P, Buvat I, Chatziioannou AF, Choi Y, Chung YH, Comtat C, Donnarieix D, Ferrer L, Glick SJ, Groiselle CJ, Guez D, Honore PF, Kerhoas-Cavata S, Kirov AS, Kohli V, Koole M, Krieguer M, van der Laan DJ, Lamare F, Largeron G, Lartizien C, Lazaro D, Maas MC, Maigne L, Mayet F, Melot F, Merheb C, Pennacchio E, Perez J, Pietrzyk U, Rannou FR, Rey M, Schaart DR, Schmidtlein CR, Simon L, Song TY, Vieira JM, Visvikis D, Van de Walle R, Wieers E, Morel C. GATE: a simulation toolkit for PET and SPECT. *Physics in Medicine & Biology* 2004; **49**(19):4543–61. DOI: 10.1088/0031-9155/49/19/007.
17. Strother SC, Casey ME, Hoffman EJ, Measuring PET. Scanner sensitivity: relating count rates to image signal-to-noise ratios using noise equivalent counts. *IEEE Transactions on Nuclear Science* 1990; **37**(2):783–788. DOI: 10.1109/23.106715.
18. Worsley KJ. Estimating the number of peaks in a random field using the Hadwiger characteristic of excursion sets, with applications to medical images. *Annals of Statistics* 1995; **23**:640–669. DOI: 10.1214/aos/1176324540.
19. Boldyš J, Dvořák J, Bělohlávek O, Skopalová M. Monte Carlo simulation of PET images for injection dose optimization. In *Proceedings of the III ECCOMAS Thematic Conference on Computational Vision and Medical Image Processing: VipIMAGE 2011*. Taylor and Francis: London, 2012.

Copyright © 2012 John Wiley & Sons, Ltd.